Journal of Radiation Research, Vol. 57, No. 6, 2016, pp. 691–701
doi: 10.1093/jrr/rrw073
Advance Access Publication: 16 August 2016

Evaluation of the radiobiological gamma index with motion interplay in tangential IMRT breast treatment

Iori Sumida[1]*, Hajime Yamaguchi[2], Indra J. Das[3], Hisao Kizaki[2], Keiko Aboshi[2], Mari Tsujii[2], Yuji Yamada[2], Kiesuke Tamari[1], Osamu Suzuki[1], Yuji Seo[1], Fumiaki Isohashi[1], Yasuo Yoshioka[1] and Kazuhiko Ogawa[1]

[1]Department of Radiation Oncology, Osaka University Graduate School of Medicine, 2-2 Yamada-oka, Suita, Osaka 565-0871, Japan
[2]Department of Radiation Oncology, NTT West Osaka Hospital, 2-6-40 Karasugatsuji, Tennoji-ku, Osaka 543-8922, Japan
[3]Department of Radiation Oncology, New York University Medical Center, 160 E, 34th Street, New York, NY 10016, USA
*Corresponding author. Department of Radiation Oncology, Osaka University Graduate School of Medicine, 2-2 Yamada-oka, Suita, Osaka 565-0871, Japan. Tel: +81-6-6879-3482; Fax: +81-6-6879-3489; Email: sumida@radonc.med.osaka-u.ac.jp
Received January 20, 2016; Revised April 6, 2016; Accepted June 1, 2016

ABSTRACT

The purpose of this study was to evaluate the impact of the motion interplay effect in early-stage left-sided breast cancer intensity-modulated radiation therapy (IMRT), incorporating the radiobiological gamma index (RGI). The IMRT dosimetry for various breathing amplitudes and cycles was investigated in 10 patients. The predicted dose was calculated using the convolution of segmented measured doses. The physical gamma index (PGI) of the planning target volume (PTV) and the organs at risk (OAR) was calculated by comparing the original with the predicted dose distributions. The RGI was calculated from the PGI using the tumor control probability (TCP) and the normal tissue complication probability (NTCP). The predicted mean dose and the generalized equivalent uniform dose (gEUD) to the target with various breathing amplitudes were lower than the original dose ($P < 0.01$). The predicted mean dose and gEUD to the OARs with motion were higher than for the original dose to the OARs ($P < 0.01$). However, the predicted data did not differ significantly between the various breathing cycles for either the PTV or the OARs. The mean RGI gamma passing rate for the PTV was higher than that for the PGI ($P < 0.01$), and for OARs, the RGI values were higher than those for the PGI ($P < 0.01$). The gamma passing rates of the RGI for the target and the OARs other than the contralateral lung differed significantly from those of the PGI under organ motion. Provided an NTCP value <0.05 is considered acceptable, it may be possible, by taking breathing motion into consideration, to escalate the dose to achieve the PTV coverage without compromising the TCP.

KEYWORDS: IMRT, quality assurance, dose prediction, radiobiological gamma index

INTRODUCTION

For left-breast cancer treatment, intensity-modulated radiation therapy (IMRT) has enabled homogeneous dose distribution to the target volume while reducing radiation-related toxicities to the heart and lungs [1–9]. Even with small breast volumes, IMRT has improved dose distribution compared with traditional treatments [10]. Cardiac and associated left anterior descending coronary artery (LAD) toxicities are directly associated with the radiation dose [11–13]. The cardiac dose can be reduced through irradiation with a deep inspiration breath-hold technique and IMRT [14, 15]. Relative to free-breathing techniques [16, 17], Colgan *et al.* [18] reported that irradiation under voluntary breath-holding is a safe technique for cardiac dose sparing.

Breast motion combined with multileaf collimator (MLC) leaf motion results in an interplay effect that causes dose blurring [19]. Frazier *et al.* [16] evaluated relevant dose–volume indices with organ motion under normal breathing in two opposed techniques, tangential and IMRT, and found the dose delivered to the breast to

be relatively insensitive to the effect of organ motion. Using 4D CT, Wang *et al.* [20] also reported that the effect of breast volume change during free breathing can be ignored and showed a correlation between the dosimetric impact and the motion of the target.

In recent years, measurement-guided dose reconstruction (MGDR) proposed by Zhen *et al.* [21] has been used and modified [22]. This approach can predict patient dose by incorporating the relative dose difference between the planned and measured data into the planned dose grid in the Digital Imaging and Communications in Medicine (DICOM) RT-dose format without recalculation of the dose in the treatment planning system (TPS).

Even with a passing rate for per-beam of >95% in IMRT quality assurance (QA), this did not always correlate with actual dose error [23]. However, it provided confidence in clinically relevant dose–volume indices with the support of dose prediction software [24]. A clinically relevant radiobiological gamma index (RGI), based on the physical gamma index [25] (PGI), has been proposed, which incorporates tumor control probability (TCP) and normal tissue complication probability (NTCP) in order to evaluate dose in both physical and clinical aspects [26]. Thus, the RGI and the PGI passing rates can act as indicators for the quality of dose delivery. However, calculating the RGI from the PGI requires the weight factor derived from the predicted dose to be specified for each voxel for both target and normal tissues. It was found that, particularly for the voxels in the target, even if the predicted dose differed from the tolerated dose (such as the prescription dose), the RGI exceeded the PGI, implying a lower passing rate for the RGI [26]. In actual cases, it is acceptable when the predicted dose exceeds the prescription dose, because the TCP value can be higher. Therefore, the weight factor should be modified appropriately.

The purpose of this study was to estimate the dosimetric impact of the interplay effect due to organ motion based on the numerical simulation. This was reconstructed throughout the time duration from the per-beam QA without motion results to predict the IMRT dose in left-sided breast cancer patients under free breathing using the MGDR approach. In addition, the dosimetric impact of the interplay was evaluated using the RGI and the PGI with modification of the weight factor.

MATERIALS AND METHODS

Treatment planning

Ten left-sided early-stage breast cancer patients who had undergone breast-conserving surgery were included. CT images with 2.5 mm slice thickness were acquired under free breathing using a GE BrightSpeed CT scanner (GE Medical Systems, Milwaukee, WI). The field borders, determined clinically by the radiation oncologist, were the mid-spinal line, the mid-axillary line, the sternal notch, and 1–2 cm below the level of the infra-mammary fold. XiO (ELEKTA Instrument AB, Stockholm, Sweden) TPS was used to calculate the dose with a convolution/superposition algorithm for heterogeneity correction. A treatment plan with two tangential opposed 6 MV beams was created in fixed-gantry step-and-shoot delivery using a MLC with leaf width 10 mm at the isocenter. The minimum area and monitor units (MUs) per segment were 2×2 cm^2 and 5 MU, respectively. The clinical target volume (CTV), ipsilateral and contralateral lung, heart, and LAD were delineated according to Radiation Therapy Oncology Group guidelines [27]. The coronary artery region was defined as the superficial 1 cm region of the left anterior quarter of the heart, as described by Hong *et al.* [28]. The planning target volume for evaluation (PTV_{eval}) was created by adding a 5 mm margin to the CTV (except for 5 mm below the skin surface, due to the build-up effect) [29], and was used to optimize the dose to the target. The median and mean PTV volumes were 532cm^3 and 509 cm^3, respectively (range 214–847 cm^3). The prescription dose was 50 Gy/25 fractions to $D_{50\%}$ of the PTV_{eval}, as described by the International Commission on Radiation Units and Measurements (ICRU-83) [30]. For dose coverage to the PTV_{eval}, it was attempted to achieve a $V_{95\%}$ (volume receiving 95% of the prescription dose in the PTV_{eval}) >95%. For the ipsilateral lung, the dose constraints were 20 Gy for ≤20% and 12 Gy for ≤30% volume. The dose constraint for the heart was a maximum of 45 Gy, based on published data [31].

Creation of a relative error map

Measured and calculated dose distributions were needed to predict the dose in patients, as previously proposed [22]. The relative error map in each beam using a 2D diode array detector (MapCHECK, Sun Nuclear Corporation, Melbourne, FL) was measured at a zero-degree gantry angle, with the remaining parameters as established by the treatment plan. In the same configuration, the coronal plane dose calculated from the TPS was exported in text format. The resolutions of the planned dose grid and MapCHECK were 1×1 mm^2 and 5×5 mm^2, respectively. The relative error map was calculated from the planned and measured doses at a resolution of 5×5 mm^2 [22].

Dose reconstruction with interplay

Breathing motion was evaluated as described by George *et al.* [32]. Although the collimator angles varied between patients, the predominant axis for the MLC motion was anterior–posterior [17]. The interplay effect was evaluated based on the dose distribution of each IMRT segment delivered at a random location with a random initial phase of organ motion, as described by Bortfeld *et al.* [19]. The resultant interplay dose distribution was the convolution of the doses from all segments. To reconstruct the dose with interplay to mimic organ motion during the beam delivery, the dose distribution measured without motion was morphed with in-house software, instead of motion-based measurement using MapCHECK. The breathing motion was recorded at 16 frames per second (fps) by placing an infrared marker on the breast surface of a volunteer and using the Synchrony® Respiratory Tracking System (Accuray Inc., Sunnyvale, CA, USA). One cycle of breathing motion of 6 mm amplitude and 4 s duration (Fig. 1) was used as a reference and applied to all cases.

To calculate the dose with interplay requires the dose distribution in each segment; this was measured in each beam using MapCHECK. Figure 2 shows the process for obtaining the measured data with interplay and the relative dose error map. The corresponding dose distribution in each segment was calculated based on the DICOM RT-plan file, taking account of segment shape and

weight with respect to the total MUs. When the collimator angle of the beam was rotated, the measured dose distribution was rotated to a collimator angle of zero degrees using a 2×2 rotation matrix. The dose distribution in each segment was deposited along the MLC leaf motion according to the trajectory shown in Fig. 1. After introducing the interplay effect, the morphed data was rotated back to the original collimator angle. The measured dose $D_k(i, j)$ of the kth segment at location i, j on the diode detector was calculated as follows:

$$D_k(i,\ j) = \frac{w_k \cdot D_{\text{total}}(i,\ j)}{\sum_{k=1}^{N_s} w_k}, \tag{1}$$

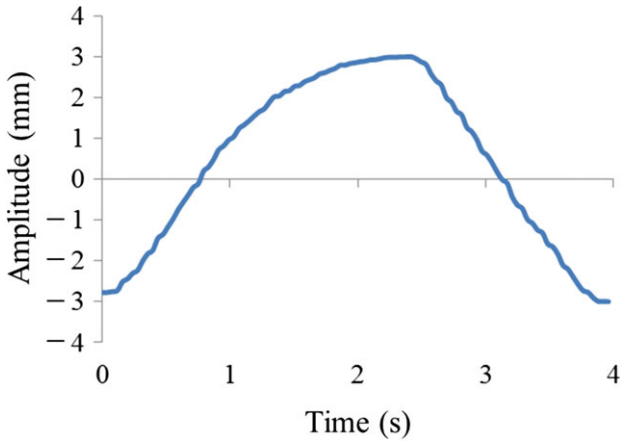

Fig. 1. A breathing motion trajectory under normal breathing.

where i and j denote the horizontal and vertical axis values of the MapCHECK at 5 mm intervals in the range −110 to +110 mm; $D_{\text{total}}(i, j)$, measured dose at location i, j in all segments; w_k, weight of the kth segment; and N_s, number of segments. If location i, j was irradiated under the closed MLC leaves, w_k was multiplied by the MLC transmission factor 0.009 (0.9%) for the 6 MV photon beam, ignoring the second-order scattered dose. As the segment dose distribution was irradiated during beam motion, the number of frames, N_f, required for delivering the dose for the kth segment was calculated as follows:

$$N_f = \frac{FR \cdot MU_k}{DR}, \tag{2}$$

where MU_k denotes MUs for segment k; FR, frame rate for recording the breathing motion (16 fps); and DR, dose rate of a 6 MV photon beam (300 MU/min). A time interval between intersegments of 0 s was assumed. The segmented dose was divided by the number of frames and deposited at the different locations according to the motion trajectory in Fig. 1. The dose distribution with interplay, $D_{\text{interplay}}(i, j)$, was calculated as follows:

$$D_{\text{interplay}}(i,\ j) = \sum_{k=1}^{N_s} \left(\sum_{l=1}^{N_f} D_{k,l}(i + x_{\text{initial frame}+l},\ j) \right) \tag{3}$$

Again, as organ motion was along the direction of MLC leaf movement, the motion trajectory x along the horizontal axis was considered while vertical motion was set to zero. The range of $x_{\text{initial frame}+l}$ was the same as for the breathing amplitude. The maximum value of initial frame + l was N_f (i.e. after reaching N_f, initial frame + l restarted from the initial frame). The dose

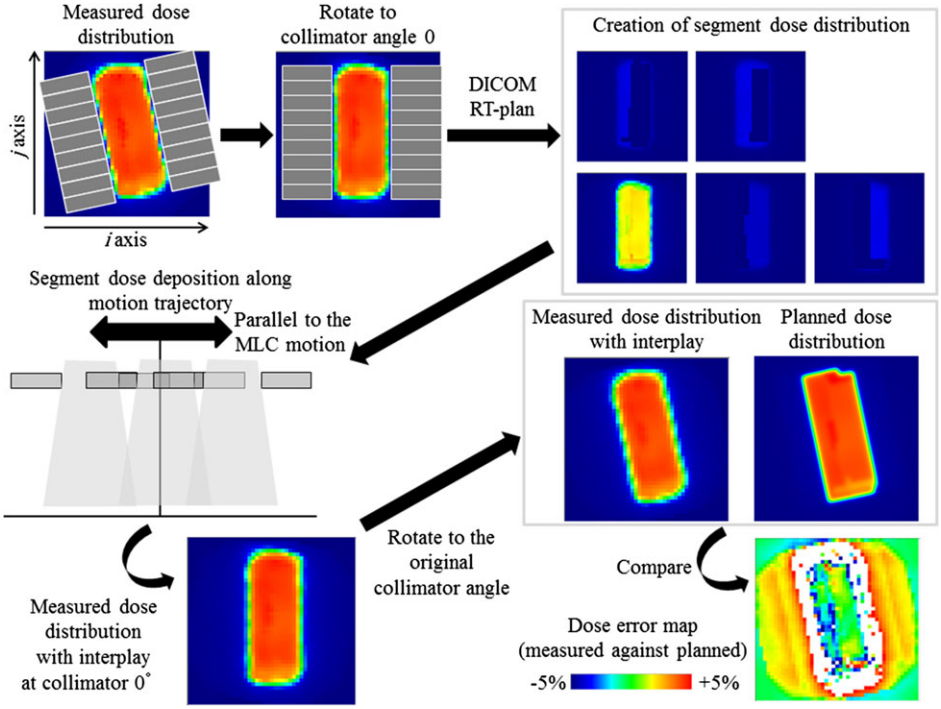

Fig. 2. Creation of the measured dose distribution with interplay and the relative dose error map.

distribution of the lth frame in the kth segment, $D_{k,l}$, was calculated as follows. First, the measured dose distribution of the kth segment was divided by N_f to obtain the dose distribution per frame. This was then deposited at locations according to the motion trajectory using 2D linear interpolation (Fig. 2). As the time to start irradiation in each segment was unknown, the initial frame number was changed randomly 1000 times to estimate the dose with interplay over the course of treatment, and the average dose distribution was calculated.

The planned dose without motion (i.e. free breathing) was used as a reference condition. To evaluate the dose with interplay under various breathing patterns, breathing amplitudes of 3, 6 and 12 mm (representing shallow, normal and deep breathing) were used, and the cycle time varied between 2, 4 and 8 s (representing fast, normal and slow cases).

Dose prediction and evaluation

The measured dose distribution was morphed according to the beam motion interplay. The relative error map between this and the planned dose was calculated and back-projected onto the planned dose to reconstruct the predicted dose based on the DICOM-RT from TPS, with a calculation grid of $1 \times 1 \times 1$ mm^3. The ray from the source to each dose grid was defined, and the intersection point on the relative dose error map located on the isocenter plane was calculated using 2D linear interpolation. The relative error was applied to each dose grid along the ray. For the dose evaluation, we calculated the mean dose and the generalized equivalent uniform dose (gEUD) in Gy, $V_{95\%}$ (%), the homogeneity index (HI), and the conformity index (CI) for the PTV_{eval}. HI was defined as $(D_{2\%} - D_{98\%})/D_{50\%}$, as discussed in ICRU-83 [30]. The CI proposed by Paddick [33] was calculated as follows:

$$\mathrm{CI} = \frac{VT_{\mathrm{pres}}}{VT} \cdot \frac{VT_{\mathrm{pres}}}{V_{\mathrm{pres}}}, \tag{4}$$

where VT_{pres} denotes target volume covered by the 95% isodose line; VT, volume of the target; and V_{pres}, treated volume covered by the 95% isodose line. The mean dose, $D_{2\%}$, gEUD in Gy, and $V_{25\mathrm{Gy}}$ (%) were calculated for the heart. Apart from the gEUD, these indices were calculated for the LAD. For the ipsilateral and contralateral lungs, the mean dose, gEUD, $V_{2\mathrm{Gy}}$, $V_{5\mathrm{Gy}}$ and $V_{20\mathrm{Gy}}$ were calculated. The gEUD was calculated for each organ using Niemierko's phenomenological formula as follows [34]:

$$\mathrm{gEUD} = \left(\frac{1}{N} \sum_{i=1}^{N} D_i^a \right)^{\frac{1}{a}}, \tag{5}$$

where N is the number of voxels in each organ, and a is a tumor or normal tissue-specific dose–volume effect parameter. For radiobiological evaluation, the individual voxel TCP was calculated using Niemierko's EUD-based model as follows [35]:

$$\mathrm{gEUD} = \left(\frac{1}{N} \sum_{i=1}^{N} D_i^a \right)^{\frac{1}{a}}, \tag{6}$$

where D_i denotes the dose delivered to the ith voxel; TCD_{50}, the dose required to achieve 50% TCP; and γ50, the normalized tumor dose–response slope at TCD_{50}. In contrast, the individual voxel NTCP was calculated using the relative seriality model [36] as follows:

$$P(D_i) = 2^{-e^{e\gamma 50\left(1-\frac{D_i}{D_{50}}\right)}}, \tag{7}$$

where D_{50} denotes the dose required to achieve 50% NTCP, and γ50 is the normalized normal tissue dose–response slope at D_{50}. The NTCP for an organ incorporating the functional architecture of relative seriality was calculated as follows:

$$P = \left[1 - \prod_{1}^{n} \left[1 - P(D_i)^s \right]^{\Delta v_i} \right]^{\frac{1}{s}}, \tag{8}$$

where n denotes the number of subvolumes in the organ; s, the relative seriality factor (ranging between 1 for a serial organ and 0 for a parallel organ); and Δv_i is defined as v_i/V, where v_i denotes the subvolume in the differential dose–volume histogram, and V denotes the total volume of the organ. These parameters for calculating the TCP and the NTCP with the endpoints in each structure are summarized in Table 1. The mean dose for the lung is equal to the gEUD due to the same tissue-specific parameter.

Table 1. Radiobiological parameters used to calculate the generalized equivalent uniform dose, tumor control probability, and normal tissue complication probability

Structure	Endpoint	Tissue-specific parameter	TCD50/D50 (Gy)	γ50	s	Study (Ref)
PTV_{eval}	Local control	−7.2	30.89	1.3		[50, 51]
Heart	Late cardiac mortality	3	52.3	1.28	1	[46]
Lung	Pneumonitis	1	26.16	0.973	0.012	[52]

TCD50 = dose required for 50% probability of tumor control, D50 = dose required for 50% probability of normal tissue complication, γ50 = slope at the TCD50 or D50, s = relative seriality factor, PTV_{eval} = planning target volume for evaluation.

The RGI [26] was calculated from PGI, briefly as follows:

$$\text{Radiobiological gamma index } (RGI) = \text{Physical gamma index } (PGI) \cdot n, \tag{9}$$

where n is the weight factor defined in Eq. 10. The PGI between the planned and predicted dose was calculated in each voxel for the criterion 3% global dose difference and 3 mm distance to agreement (3% global/3 mm). For voxels with a PGI of 1 and over, the TCP and NTCP values with the predicted dose were calculated, and the weight factor n was calculated as follows:

$$n = \begin{cases} 1 \pm |\text{TCP}_i - \text{Tolerated TCP}|, \text{ for the target} \\ 1 + (\text{NTCP}_i - \text{Tolerated NTCP}), \text{ for the normal tissue,} \end{cases} \tag{10}$$

where TCP_i and NTCP_i are values at the ith voxel in the predicted dose. Clinically acceptable values assumed when calculating the RGI were a tolerated TCP of 0.924 (a value derived from the mean value of all clinical approved plans) and a tolerated NTCP of 0.05 (derived from the tolerated dose TD5/5, i.e. NTCP at 5% within 5 years after radiotherapy and reported as good treatment [37]), although those tolerated values depend on the tissues. For the target, when the predicted dose of the ith voxel is <95% of the prescription dose, the factor n exceeds 1, which means $n = 1 + |\text{TCP}_i - \text{Tolerated TCP}|$, and so the RGI is greater than the PGI. Conversely, when the predicted dose of the ith voxel exceeds 95% of the prescription dose, n is less than 1, which means $n = 1 - |\text{TCP}_i - \text{Tolerated TCP}|$, and the RGI is less than the PGI. The acceptable lower threshold of 95% was recommended in ICRU Report 50 [38]. For the normal tissue, the predicted dose is preferably as low as possible; therefore, n is less than 1 when NTCP_i is lower than the tolerated NTCP. The gamma passing rates of the PGI and the RGI were calculated for each organ. Correlations between the passing rates of the RGI with various breathing amplitudes and the predicted dose–volume indices for organs were evaluated.

Statistical analysis

The normality of the data was checked with the Shapiro–Wilk test, and comparison analysis used the two-tailed paired t-test or the Wilcoxon signed-rank test as appropriate. For correlation analysis, either Pearson's or Spearman's correlation coefficient (r) was selected according to the normality. A P-value <0.05 was considered statistically significant. Statistical analyses were performed using R version 3.1.2 statistical software (R Foundation, Vienna, Austria).

RESULTS

Tables 2 and 3 summarize the dose–volume indices, comparing the original dose and the predicted dose with interplay. In Table 2, the breathing patterns combine three different amplitudes (shallow, normal and deep) with the normal breathing cycle time. For the heart, the values for mean dose, $D_{2\%}$ and gEUD with motion were significantly greater than those for the original dose ($P < 0.01$ or 0.05, respectively). The NTCP values for the motion data under deep breathing were marginally higher than those for the original data ($P < 0.01$). Other breathing amplitudes did not differ significantly. V_{25Gy} for the motion data were significantly greater than those for the original data ($P < 0.01$). The larger amplitudes resulted in higher volume indices. For LAD, the mean doses with motion were greater than those for the original data ($P < 0.01$). The V_{25Gy} were 12.4%, 14.4%, 15.5% and 18.1% for original, shallow, normal and deep breathing amplitudes, respectively ($P < 0.01$). However, the $D_{2\%}$ for the motion data did not differ significantly from those for the original data, possibly due to averaging over time. For the right lung, the mean dose (gEUD) with motion was significantly greater than that for the original data ($P < 0.01$), although the difference was small (0.05 Gy). For the left lung, all motion parameters were greater than those for the original data ($P < 0.01$). V_{2Gy}, V_{5Gy} and V_{20Gy} with motion were around 16%, 8% and 3–5% higher than those of the original data, respectively. For PTV_{eval}, the mean dose and gEUD values gradually decreased with increasing amplitudes, with a difference of ~1 Gy. The TCPs with motion were also reduced from the original data ($P < 0.01$). The $V_{95\%}$ values were 98.8%, 91.9%, 90.3% and 85.2% for original, shallow, normal and deep breathing amplitudes, respectively ($P < 0.01$). The CI with motion was not significantly different from that for the original data, but HI was greater.

Table 3 shows the data for breathing patterns that combined the three different cycle times (slow, normal and fast) with normal amplitude. The motion data for the normal amplitude and cycle time were the same as those in Table 2 and, therefore, showed the same tendency in differences between the predicted and original data. In particular, the predicted data were almost the same between the various cycle times. When repeated data analysis of variance (ANOVA) was performed to compare the three cycles, there were no significant differences for pairwise comparisons of the slow–normal, slow–fast or normal–fast combinations.

As the predicted data were almost the same between the various cycle times, the analysis was limited to the comparisons of passing rates between the PGIs with 3% global/3 mm criteria and the RGIs with different amplitudes (Table 4). The RGI passing rates exceeded those of the PGI ($P < 0.01$) for all OARs other than the right lung, where the RGI and PGI passing rates were similar. For PTV_{eval}, the RGI passing rates also exceeded those of PGI for each breathing pattern ($P < 0.01$), even though the TCP values decreased from the original data to the motion data. The maximum differences between RGI and PGI with the 3% global/3 mm criterion were 1.1%, 1.1% and 0.3% in the heart, left lung and PTV_{eval}, respectively.

Significant negative correlations were found between the RGI passing rates and the $D_{2\%}$ and V_{25Gy} for the heart under deep breathing amplitude ($P = 0.01$ and 0.04, respectively) (Fig. 3 and Table 5). Positive correlations were found between the RGI passing rates and the mean dose under normal and deep breathing amplitudes, gEUD under shallow, normal and deep breathing amplitudes, and TCP under shallow, normal and deep breathing amplitudes (all $P = 0.02$). Other combinations of the RGI passing rates and predicted dose–volume indices did not differ significantly.

DISCUSSION

The predicted dose obtained from the MGDR approach took account of machine errors for dose delivery, such as the deviation of

Table 2. Comparisons between the original and predicted dose–volume indices with a normal breathing cycle at various amplitudes

			Amplitude		
Organ	Index	Original	Shallow	Normal	Deep
Heart	Mean dose (Gy)	1.77 ± 0.85	2.52 ± 0.99*	2.57 ± 1.01*	2.70 ± 1.07*
	$D_{2\%}$ (Gy)	19.52 ± 14.70	22.17 ± 14.48**	22.85 ± 14.60**	24.32 ± 14.52**
	gEUD (Gy)	8.23 ± 4.69	8.78 ± 4.35**	8.98 ± 4.29**	9.54 ± 4.19*
	NTCP	0.0034 ± 0.0033	0.0035 ± 0.0032	0.0035 ± 0.0032	0.0038 ± 0.0035*
	V_{25Gy} (%)	1.58 ± 1.40	1.95 ± 1.67*	2.12 ± 1.77*	2.53 ± 2.00*
LAD	Mean dose (Gy)	8.31 ± 4.99	9.99 ± 5.21*	10.30 ± 5.31*	11.13 ± 5.56*
	$D_{2\%}$ (Gy)	33.08 ± 17.01	33.81 ± 14.38	34.06 ± 13.31	35.06 ± 11.47
	V_{25Gy} (%)	12.39 ± 10.76	14.37 ± 11.94*	15.53 ± 12.60*	18.13 ± 13.96*
Right lung	Mean dose = gEUD (Gy)	0.14 ± 0.03	0.19 ± 0.04*	0.19 ± 0.04*	0.19 ± 0.04*
	NTCP	0.0001 ± 0.0000	0.0001 ± 0.0000	0.0001 ± 0.0000	0.0001 ± 0.0000
	V_{2Gy} (%)	0.00 ± 0.01	0.13 ± 0.28	0.13 ± 0.28	0.14 ± 0.31
	V_{5Gy} (%)	0.00 ± 0.00	0.00 ± 0.00	0.00 ± 0.00	0.00 ± 0.00
	V_{20Gy} (%)	0.00 ± 0.00	0.00 ± 0.00	0.00 ± 0.00	0.00 ± 0.00
Left lung	Mean dose = gEUD (Gy)	4.78 ± 1.81	5.73 ± 1.80*	5.85 ± 1.79*	6.17 ± 1.78*
	NTCP	0.0053 ± 0.0071	0.0117 ± 0.0141*	0.0122 ± 0.0144*	0.0138 ± 0.0150*
	V_{2Gy} (%)	29.31 ± 4.82	45.38 ± 8.53*	45.28 ± 8.39*	45.25 ± 8.20*
	V_{5Gy} (%)	17.75 ± 4.67	25.50 ± 5.32*	25.57 ± 5.27*	26.00 ± 5.18*
	V_{20Gy} (%)	9.68 ± 4.18	12.92 ± 4.70*	13.64 ± 4.73*	15.12 ± 4.75*
PTV_{eval}	Mean dose (Gy)	50.06 ± 0.04	49.29 ± 0.17*	49.19 ± 0.19*	48.89 ± 0.25*
	gEUD (Gy)	49.98 ± 0.05	49.05 ± 0.28*	48.91 ± 0.32*	48.44 ± 0.43*
	TCP	0.9243 ± 0.0004	0.9171 ± 0.0023*	0.9160 ± 0.0027*	0.9120 ± 0.0038*
	$V_{95\%}$ (%)	98.84 ± 1.50	91.94 ± 3.28*	90.33 ± 3.17*	85.19 ± 2.86*
	CI	0.63 ± 0.12	0.62 ± 0.09	0.62 ± 0.09	0.61 ± 0.09
	HI	0.08 ± 0.02	0.12 ± 0.03*	0.13 ± 0.03*	0.16 ± 0.03*

LAD = left anterior descending coronary artery, PTV_{eval} = planning target volume for evaluation, gEUD = generalized equivalent uniform dose, NTCP = normal tissue complication probability, TCP = tumor control probability, CI = conformity index, HI = homogeneity index, $D_{2\%}$ = the absorbed dose received by 2% of the volume, V_{xGy} = the percentage of volume receiving x Gy. Values are means ± SD. *$P < 0.01$, **$P < 0.05$ (statistically significant difference from the original data).

MLC leaf position, beam output, and stability of the measurement device. It is useful to evaluate dose in close-to-actual radiation treatment; therefore, we made dosimetric comparisons between planned and predicted doses. This MGDR approach does not need dose recalculation in the TPS, so it is important that accurate beam modeling characterization in TPS is based on an accurate measured dose distribution. It should be noted that even though the predicted doses are close to those of actual radiation treatment, the dosimetric results presented in this simulation study are not always applicable to the actual treatment. Thus, the dosimetric results should be evaluated and confirmed by future clinical studies.

The dose distribution with motion interplay can be calculated based on the static dose in each segment, as described by Li *et al.* [39]. George *et al.* [32] reproduced this by changing the MLC leaf sequence. We have presented an alternative approach, based on the individual segmented dose from the measured data using the DICOM RT-plan file without motion, taking advantage of not needing to recalculate the dose in the TPS to estimate the interplay

Table 3. Comparisons between the original and the predicted dose–volume indices at normal amplitude with different breathing cycles

Organ	Index	Original	Cycle		
			Slow	Normal	Fast
Heart	Mean dose (Gy)	1.77 ± 0.85	2.57 ± 1.01*	2.57 ± 1.01*	2.57 ± 1.01*
	$D_{2\%}$ (Gy)	19.52 ± 14.70	22.85 ± 14.60**	22.85 ± 14.60**	22.85 ± 14.59**
	gEUD (Gy)	8.23 ± 4.69	8.98 ± 4.29**	8.98 ± 4.29**	8.98 ± 4.29**
	NTCP	0.0034 ± 0.0033	0.0035 ± 0.0032	0.0035 ± 0.0032	0.0035 ± 0.0032
	V_{25Gy} (%)	1.58 ± 1.40	2.12 ± 1.77*	2.12 ± 1.77*	2.12 ± 1.77*
LAD	Mean dose (Gy)	8.31 ± 4.99	10.31 ± 5.31*	10.30 ± 5.31*	10.30 ± 5.31*
	$D_{2\%}$ (Gy)	33.08 ± 17.01	34.07 ± 13.31	34.06 ± 13.31	34.06 ± 13.31
	V_{25Gy} (%)	12.39 ± 10.76	15.53 ± 12.59*	15.53 ± 12.60*	15.53 ± 12.60*
Right lung	Mean dose = gEUD (Gy)	0.14 ± 0.03	0.19 ± 0.04*	0.19 ± 0.04*	0.19 ± 0.04*
	NTCP	0.0001 ± 0.0000	0.0001 ± 0.0000	0.0001 ± 0.0000	0.0001 ± 0.0000
	V_{2Gy} (%)	0.00 ± 0.01	0.13 ± 0.28	0.13 ± 0.28	0.13 ± 0.28
	V_{5Gy} (%)	0.00 ± 0.00	0.00 ± 0.00	0.00 ± 0.00	0.00 ± 0.00
	V_{20Gy} (%)	0.00 ± 0.00	0.00 ± 0.00	0.00 ± 0.00	0.00 ± 0.00
Left lung	Mean dose = gEUD (Gy)	4.78 ± 1.81	5.85 ± 1.79*	5.85 ± 1.79*	5.85 ± 1.79*
	NTCP	0.0053 ± 0.0071	0.0122 ± 0.0144*	0.0122 ± 0.0144*	0.0122 ± 0.0144*
	V_{2Gy} (%)	29.31 ± 4.82	45.28 ± 8.39*	45.28 ± 8.39*	45.28 ± 8.39*
	V_{5Gy} (%)	17.75 ± 4.67	25.57 ± 5.27*	25.57 ± 5.27*	25.57 ± 5.27*
	V_{20Gy} (%)	9.68 ± 4.18	13.65 ± 4.72*	13.64 ± 4.73*	13.64 ± 4.73*
PTV_{eval}	Mean dose (Gy)	50.06 ± 0.04	49.19 ± 0.20*	49.19 ± 0.19*	49.20 ± 0.20*
	gEUD (Gy)	49.98 ± 0.05	48.91 ± 0.33*	48.91 ± 0.32*	48.91 ± 0.33*
	TCP	0.9243 ± 0.0004	0.9160 ± 0.0027*	0.9160 ± 0.0027*	0.9160 ± 0.0027*
	$V_{95\%}$ (%)	98.84 ± 1.50	90.31 ± 3.14*	90.33 ± 3.17*	90.37 ± 3.03*
	CI	0.63 ± 0.12	0.62 ± 0.09	0.62 ± 0.09	0.62 ± 0.09
	HI	0.08 ± 0.02	0.13 ± 0.03*	0.13 ± 0.03*	0.13 ± 0.03*

LAD = left anterior descending coronary artery, PTV_{eval} = planning target volume for evaluation, gEUD = generalized equivalent uniform dose, NTCP = normal tissue complication probability, TCP = tumor control probability, CI = conformity index, HI = homogeneity index, $D_{2\%}$ = the absorbed dose received by 2% of the volume, V_{xGy} = the percentage of volume receiving *x* Gy. Values are means ± SD. *$P < 0.01$, **$P < 0.05$ (statistically significant difference from the original data).

effect. However, the detector density of the MapCHECK was coarse (5 mm with respect to the motion amplitude used in this study); in future, the finer detector density of an electric portal imaging device or the doubled detector density method [40] of the MapCHECK should be used. It will be important to evaluate the dose in the MLC leaf penumbra region for interplay, particularly for the LAD because of its relatively small volume compared with that of other organs. Another limitation of this study is that the relative dose error map used to predict the dose was measured by the MapCHECK device at gantry 0, a different gantry angle than that used during actual treatment. Sumida *et al.* [41] reported the effect of significant dosimetric impact at the MLC leaf abutment in step-and-shoot IMRT on the prediction of dose according to the difference in gantry angles between measurement and actual treatment. The same type of double-focused MLC leaf was used as in the present study, and from their data, an estimate of the leaf opening errors at the gantry angle of left-sided tangential irradiation, compared with the gantry 0, would be ~0.5 mm [41]. There may be

Table 4. Comparisons between the passing rates of the physical gamma index (3%/3 mm tolerance) and radiobiological gamma index of each organ in 10 patients

Organ	Amplitude	PGI (%)	RGI (%)	*P* value
Heart	Shallow	93.67 ± 5.77	94.36 ± 5.44	<0.01
	Normal	93.16 ± 5.53	93.98 ± 5.23	<0.01
	Deep	89.64 ± 5.23	90.70 ± 4.99	<0.01
Right lung	Shallow	54.33 ± 2.21	54.33 ± 2.21	NS
	Normal	54.36 ± 2.19	54.36 ± 2.19	NS
	Deep	54.28 ± 2.12	54.28 ± 2.12	NS
Left lung	Shallow	74.54 ± 4.59	75.60 ± 4.44	<0.01
	Normal	73.06 ± 4.31	74.07 ± 4.11	<0.01
	Deep	68.93 ± 3.87	69.80 ± 3.72	<0.01
PTV_{eval}	Shallow	92.95 ± 2.52	93.08 ± 2.50	<0.01
	Normal	90.29 ± 3.14	90.47 ± 3.10	<0.01
	Deep	81.80 ± 4.57	82.06 ± 4.47	<0.01

PGI = physical gamma index, RGI = radiobiological gamma index, PTV_{eval} = planning target volume for evaluation, NS = not significant. Values are means ± SD.

significant dosimetric impact on organ dose evaluation, which should be taken into consideration in future studies.

A novel finding of the present study was that the original and motion data are independent of the duration of the breathing cycle, but dependent on the amplitude. For the same amplitude but different cycle times, the dose–volume indices were almost the same, as was shown by Chui *et al.* [17]. Taylor *et al.* [42] reported doses of 2.3 ± 0.7 Gy and 7.6 ± 4.5 Gy to the heart and LAD, respectively, for left-sided tangential irradiation and concluded that the mean heart dose was ~2 Gy. Jin *et al.* [4] reported a mean heart dose of 2.2 Gy for tangential IMRT. In the present study, the mean heart doses in the original dose and predicted dose with deep amplitude were 1.8 Gy and 2.7 Gy, respectively. According to Darby *et al.* [11], major coronary event rates increased linearly with the mean dose to the heart by 7.4% per Gy. Attention should therefore be given to the increased mean heart dose with larger amplitude.

Chui *et al.* [17] reported penumbral broadening with organ motion during IMRT irradiation for breast cancer. This produces a higher dose outside and near the field edge and a lower dose inside and near the field edge compared with the dose without motion. Our study found that greater breathing amplitudes resulted in higher doses to the OARs. For the heart and LAD, the location was mostly outside the field edge. For the lungs, the greatest volumes were outside the field, but the partial volume of the left lung was inside the field edge. This impacts the data measured using a diode array that overresponds in the low-dose regions outside the field [43] and the accuracy of the beam profile modeling, such as the off-center ratio, especially outside the field shown as the dose error map in Fig. 2. Both issues could affect the predicted dose distribution as systematic errors. Jang *et al.* [44] reported the underestimation to be <10 Gy for dose calculations in commercial TPS for lung cancer. Kim *et al.* [45] also reported that MLC scatter depends on the MLC leakage that contributes to the increased dose outside the field. Although a MLC transmission factor of 0.009 was considered to divide the segment dose distribution as primary radiation, the scattered radiation from the MLC leaf was not considered as a second-order fator in the TPS. This concern needs to be described in future studies to divide the segment dose distribution more accurately.

The beam intensity on the target side of the interface between the left lung and the PTV_{eval} is relatively high in order to irradiate a homogeneous dose to the PTV_{eval} and to reduce the dose to the left lung. When the organ moves during beam delivery, the high-intensity region partially irradiates the left lung region. This would also occur for rib bones due to their high-density material. The dose for rib bones was not evaluated in this study; however, some parts of them are located close to the surface of the patient's skin covered by the build-up region of the beam, and these parts may receive an unexpectedly high dose due to the organ motion.

Regarding the PTV_{eval}, as mentioned earlier the penumbral broadening reduces the dose to the target, in particular the $V_{95\%}$ for greater breathing amplitudes [17]. The mean HI increased from the original data of 0.08 to 0.16 with deep amplitude breathing. This means that inhomogeneity within the target increases with increasing amplitude because the $D_{98\%}$ decreases with increasing amplitude, even though the $D_{2\%}$ and $D_{50\%}$ remain almost unchanged (data not shown). This is consistent with reported data [17], although those authors used D_{min} instead of $D_{98\%}$. The mean dose for a large amplitude was 48.9 Gy, which was 1.1 Gy lower than the original data dose of 50.0 Gy. Scaling the relative reduction of 2.4% up to 50.0 Gy, the mean dose for the heart, right lung and left lung would be 2.8 Gy, 0.2 Gy and 6.3 Gy, respectively. As noted previously, major coronary event rates increase linearly with the heart mean dose by 7.4% per Gy [11]. Even assuming that the prescription dose is based on the mean dose, the NTCP for OARs would still be close to zero. However, Gagliardi *et al.* [46] recommended that the irradiated heart volume be minimized as far as possible without compromising the target coverage, especially the mean dose of the LAD, which correlates with the mean dose to the heart and which may have higher correlation with the cardiac risk [42, 47]. Rescaling the prescription dose to the target should therefore be given careful attention for doses in other normal tissues.

We evaluated the dose with interplay for the PTV_{eval} and the OARs assuming no intrafractional organ deformation during irradiation and no set-up error for the patient. Although Wang *et al.* [20] reported that the breast volume change during free breathing can be ignored and that the dosimetric impact was small, dosimetric impact with organ deformation should be evaluated further in the future. In addition, one-cycle breath motion was used as a reference in this study, focusing on the difference between breathing amplitude and cycle. Tudor *et al.* [48] reported that baseline variations during treatment cause a dosimetric impact to the target, largely due to the interplay effect. In addition, since breathing patterns vary between

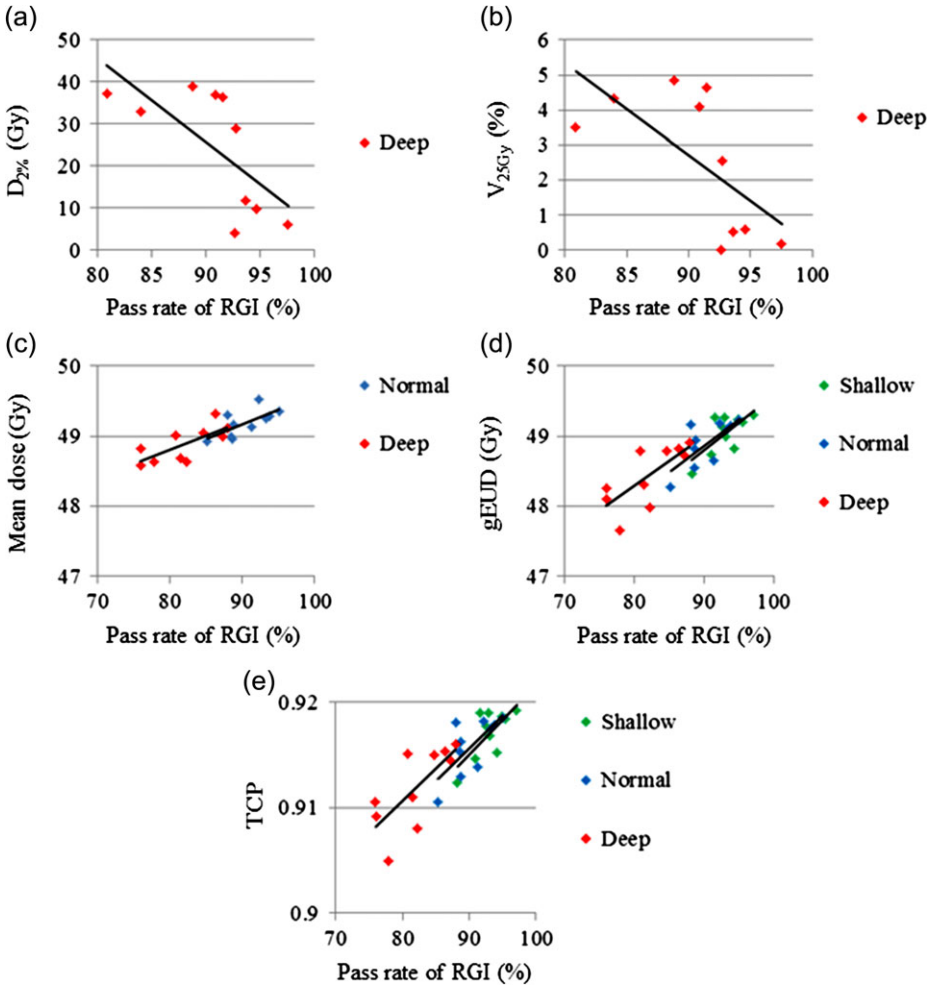

Fig. 3. Correlations between the passing rates of radiobiological gamma index and the predicted dose–volume indices. (a) $D_{2\%}$ (Gy), (b) V_{25Gy} (%) for the heart, (c) mean dose (Gy), (d) gEUD (Gy) and (e) TCP for the PTV_{eval}. The symbol colors indicate the breathing amplitude. The solid line shows linear regression.

patients, in the future other patterns as well as the baseline shift during treatment should be considered for dose evaluation with interplay. Over the course of treatment, a set-up error for the patient would have a dosimetric impact. To investigate how large the impact would be in target and normal tissues, it would, for example, be possible to change the isocenter location per fraction in this MGDR approach to estimate the differences between planned and predicted doses.

The RGI passing rates for the target and normal tissues (other than for the right lung) were higher than those for the PGI. Even if the predicted dose to the OARs under organ motion was higher than the original dose, resulting in PGI ≥ 1, when the NTCP value from the predicted dose was <0.05, the failed dose grid altered the passing dose grid. The planned dose for the OARs was sufficiently lower than the dose constraint that would lead to such a situation. In addition, even if the PGI for the target was ≥ 1 in the voxel, a voxel with a predicted dose >95% of the prescription dose would be accepted in the RGI. The probability of change in the PGI to the RGI depends on the weight factor n in Eq. 10. This factor was defined as a monotonic proportion; however, in general the TCP value is high and located at the end of the slope and at the shoulder of the TCP curve. In contrast, the NTCP is low and located at the beginning of the slope and at the bottom of the NTCP curve. The sensitivity of the change in TCP/NTCP would be different for the target and critical organ. Therefore, the weight factor n may not be monotonic, and a more appropriate alternative should be investigated in the future.

Regarding the correlation between the RGI passing rates and predicted dose–volume indices, the results showed that when the RGI passing rates decrease, $D_{2\%}$ and V_{25Gy} increase for the heart, and when the RGI passing rates decrease, the mean dose and gEUD decrease for the PTV_{eval}, which indicates that the TCP value would also decrease. The RGI provides both physical and radiobiological evaluations as well as the statistical correlation presented previously. Thus, the evaluation method using the RGI passing rates may be considered superior. However, appropriate values for obtaining

Table 5. Indices of correlation between the passing rates of radiobiological gamma index and dose–volume indices

Organ	Index	Amplitude	Correlation factor	*P* value
Heart	$D_{2\%}$ (Gy)	Deep	−0.782	0.01
	V_{25Gy} (%)		−0.648	0.04
PTV_{eval}	Mean dose (Gy)	Normal	0.704	0.02
		Deep	0.731	0.02
	gEUD	Shallow	0.708	0.02
		Normal	0.719	0.02
		Deep	0.733	0.02
	TCP	Shallow	0.707	0.02
		Normal	0.718	0.02
		Deep	0.725	0.02

$D_{2\%}$ = the absorbed dose received by 2% of the volume, V_{25Gy} = the percentage of volume receiving 25 Gy, PTV_{eval} = planning target volume for evaluation, gEUD = generalized equivalent uniform dose, TCP = tumor control probability.

more sensitive RGI values are needed as there are no statistical correlations for other organs under various breathing amplitudes.

The sensitivity of the RGI results in the gamma passing rate depends on the values of the tolerated TCP and NTCP. For late cardiac mortality, the tolerated NTCP of 0.05 was recommended in the report of Gagliardi *et al.* [46]. For radiation pneumonitis of the lung, the acceptable risk level varies with the clinical scenario [49]. Although the tolerated NTCP for the lung was set to 0.05 in this study, a physician may change the value depending on the clinical endpoint.

The effect of organ motion on left-breast dosimetry was evaluated using an MGDR approach based on the data measured without motion. Our approach is comparable with that of other published reports [32, 39]. This study showed that, for the target, the RGI passing rate was higher than that of the PGI, even though the dose coverage was worse; for OARs, it was higher than that of the PGI when organ motion was taken into consideration. Although acceptable NTCP values vary between organs and depend on a physician's judgement, provided that the NTCP value of <0.05 is considered acceptable, one option may be to scale up the dose to achieve good PTV coverage and maintain TCP. Motion results in an underdose to the target, and this should be taken into account in breast cancer treatment.

CONFLICT OF INTEREST

There is no conflict of interest to declare.

REFERENCES

1. Mahmoudzadeh H, Lee J, Chan TC, et al. Robust optimization methods for cardiac sparing in tangential breast IMRT. *Med Phys* 2015;42:2212–22.
2. Roberts KB, Soulos PR, Herrin J, et al. The adoption of new adjuvant radiation therapy modalities among Medicare beneficiaries with breast cancer: clinical correlates and cost implications. *Int J Radiat Oncol Biol Phys* 2013;85:1186–92.
3. Smith BD, Pan IW, Shih YC, et al. Adoption of intensity-modulated radiation therapy for breast cancer in the United States. *J Natl Cancer Inst* 2011;103:798–809.
4. Jin G-H, Chen L-X, Deng X-W, et al. A comparative dosimetric study for treating left-sided breast cancer for small breast size using five different radiotherapy techniques: conventional tangential field, filed-in-filed, tangential-IMRT, multi-beam IMRT and VMAT. *Radiat Oncol* 2013;8:89–97.
5. Keller LM, Sopka DM, Li T, et al. Five-year results of whole breast intensity modulated radiation therapy for the treatment of early stage breast cancer: the Fox Chase Cancer Center experience. *Int J Radiat Oncol Biol Phys* 2012;84:881–7.
6. Jeulink M, Dahele M, Meijnen P, et al. Is there a preferred IMRT technique for left-breast irradiation? *J Appl Clin Med Phys* 2015;16:5266.
7. Smith W, Menon G, Wolfe N, et al. IMRT for the breast: a comparison of tangential planning techniques. *Phys Med Biol* 2010;55:1231–41.
8. Freedman GM, Li T, Nicolaou N, et al. Breast intensity-modulated radiation therapy reduces time spent with acute dermatitis for women of all breast sizes during radiation. *Int J Radiat Oncol Biol Phys* 2009;74:689–94.
9. Harsolia A, Kestin L, Grills I, et al. Intensity-modulated radiotherapy results in significant decrease in clinical toxicities compared with conventional wedge-based breast radiotherapy. *Int J Radiat Oncol Biol Phys* 2007;68:1375–80.
10. Tsuchiya K, Kinoshita R, Shimizu S, et al. Dosimetric comparison between intensity-modulated radiotherapy and standard wedged tangential technique for whole-breast radiotherapy in Asian women with relatively small breast volumes. *Radiol Phys Technol* 2014;7:67–72.
11. Darby SC, Ewertz M, McGale P, et al. Risk of ischemic heart disease in women after radiotherapy for breast cancer. *N Engl J Med* 2013;368:987–98.
12. Shah C, Badiyan S, Berry S, et al. Cardiac dose sparing and avoidance techniques in breast cancer radiotherapy. *Radiother Oncol* 2014;112:9–16.
13. Beck RE, Kim L, Yue NJ, et al. Treatment techniques to reduce cardiac irradiation for breast cancer patients treated with breast-conserving surgery and radiation therapy: a review. *Front Oncol* 2014;4:327.
14. Hayden AJ, Rains M, Tiver K. Deep inspiration breath hold technique reduces heart dose from radiotherapy for left-sided breast cancer. *J Med Imaging Radiat Oncol* 2012;56:464–72.
15. Wang W, Purdie TG, Rahman M, et al. Rapid automated treatment planning process to select breast cancer patients for active breathing control to achieve cardiac dose reduction. *Int J Radiat Oncol Biol Phys* 2012;82:386–93.
16. Frazier RC, Vicini FA, Sharpe MB, et al. Impact of breathing motion on whole breast radiotherapy: a dosimetric analysis using active breathing control. *Int J Radiat Oncol Biol Phys* 2004;58:1041–7.

17. Chui CS, Yorke E, Hong L. The effects of intra-fraction organ motion on the delivery of intensity-modulated field with a multileaf collimator. *Med Phys* 2003;30:1736–46.
18. Colgan R, James M, Bartlett FR, et al. Voluntary breath-holding for breast cancer radiotherapy is consistent and stable. *Br J Radiol* 2015;88:309–317.
19. Bortfeld T, Jiang SB, Rietzel E. Effects of motion on the total dose distribution. *Semin Radiat Oncol* 2004;14:41–51.
20. Wang W, Li JB, Hu HG, et al. Correlation between target motion and the dosimetric variance of breast and organ at risk during whole breast radiotherapy using 4DCT. *Radiat Oncol* 2013;8:111–6.
21. Zhen H, Nelms BE, Tomé WA. Moving from gamma passing rates to patient DVH-based QA metrics in pretreatment dose QA. *Med Phys* 2011;38:5477–89.
22. Sumida I, Yamaguchi H, Kizaki H, et al. Three-dimensional dose prediction based on two-dimensional verification measurements for IMRT. *J Appl Clin Med Phys* 2014;15:4874.
23. Nelms BE, Zhen H, Tomé WA. Per-beam, planar IMRT QA passing rates do not predict clinically relevant patient dose errors. *Med Phys* 2011;38:1037–44.
24. Stasi M, Bresciani S, Miranti A, et al. Pretreatment patient-specific IMRT quality assurance: a correlation study between gamma index and patient clinical dose volume histogram. *Med Phys* 2012;39:7626–34.
25. Low DA, Harms WB, Mutic S, et al. A technique for the quantitative evaluation of dose distributions. *Med Phys* 1998;25:656–61.
26. Sumida I, Yamaguchi H, Kizaki H, et al. Novel radiobiological gamma index for evaluation of 3-dimensional predicted dose distribution. *Int J Radiat Oncol Biol Phys* 2015;92:779–86.
27. RTOG. *Breast Cancer Atlas for Radiation Therapy Planning: Consensus Definitions.* http://www.rtog.org/CoreLab/ContouringAtlases/BreastCancerAtlas.aspx (18 June 2013, date last accessed).
28. Hong L, Hunt M, Chui C, et al. Intensity-modulated tangential beam irradiation of the intact breast. *Int J Radiat Oncol Biol Phys* 1999;44:1155–64.
29. NSABP and RTOG. NSABP protocol B-39. RTOG protocol 0413. A randomized Phase III study of conventional whole breast irradiation (WBI) versus partial breast irradiation (PBI) for women with Stage 0, I, or II breast cancer. Philadelphia: RTOG, March 13, 2007, 122 pp.
30. International Commission on Radiation Units and Measurements. Prescribing, recording and reporting photon-beam intensity-modulated radiation therapy (IMRT). Special considerations regarding absorbed-dose and dose–volume prescribing and reporting in IMRT. ICRU Report 83. *J ICRU* 2010;10:27–40.
31. Rudat V, Nour A, Alaradi AA, et al. *In vivo* surface dose measurement using GafChromic film dosimetry in breast cancer radiotherapy: comparison of 7-field IMRT, tangential IMRT and tangential 3D-CRT. *Radiat Oncol* 2014;9:156–65.
32. George R, Keall PJ, Kini VR, et al. Quantifying the effect of intrafraction motion during breast IMRT planning and dose delivery. *Med Phys* 2003;30:552–62.
33. Paddick I. A simple scoring ratio to index the conformity of radiosurgical treatment plans. Technical note. *J Neurosurg* 2000;93 Suppl 3:219–22.
34. Wu Q, Mohan R, Niemierko A, et al. Optimization of intensity-modulated radiotherapy plans based on the equivalent uniform dose. *Int J Radiat Oncol Biol Phys* 2002;52:224–35.
35. Kim Y, Tomé WA. Risk-adaptive optimization: selective boosting of high-risk tumor subvolumes. *Int J Radiat Oncol Biol Phys* 2006;66:1528–42.
36. Källman P, Ågren A, Brahme A. Tumour and normal tissue responses to fractionated non-uniform dose delivery. *Int J Radiat Biol* 1992;62:249–62.
37. Suntharalingam N, Podgorsak EB, Hendry JH. Basic radiobiology. In: Podgorsak EB (ed). *Radiation Oncology Physics.* Vienna, Austria: International Atomic Energy Agency, 2005, 485–504.
38. International Commission on Radiation Units and Measurements. Prescribing, Recording and Reporting Photon Beam Therapy, 2nd edn. *ICRU Report No. 50.* International Commission on Radiation Units and Measurements, Bethesda, MD, 1993.
39. Li HS, Chetty IJ, Solberg TD. Quantifying the interplay effect in prostate IMRT delivery using a convolution-based method. *Med Phys* 2008;35:1703–10.
40. Keeling VP, Ahmad S, Algan O, et al. Dependency of planned dose perturbation (PDP) on the spatial resolution of MapCHECK 2 detectors. *J Appl Clin Med Phys* 2014;15:4457.
41. Sumida I, Yamaguchi H, Kizaki H, et al. Incorporation of gantry angle correction for 3D dose prediction in intensity-modulated radiation therapy. *J Radiat Res* 2015;56:594–605.
42. Taylor CW, Povall JM, McGale P, et al. Cardiac dose from tangential breast cancer radiotherapy in the year 2006. *Int J Radiat Oncol Biol Phys* 2008;72:501–7.
43. Low DA, Moran JM, Dempsey JF, et al. Dosimetry tools and techniques for IMRT. *Med Phys* 2011;38:1313–38.
44. Jang SY, Liu HH, Mohan R. Underestimation of low-dose radiation in treatment planning of intensity-modulated radiotherapy. *Int J Radiat Oncol Biol Phys* 2008;71:1537–46.
45. Kim JO, Siebers JV, Keall PJ, et al. A Monte Carlo study of radiation transport through multileaf collimators. *Med Phys* 2001;28:2497–506.
46. Gagliardi G, Constine LS, Moiseenko V, et al. Radiation dose–volume effects in the heart. *Int J Radiat Oncol Biol Phys* 2010;76:S77–85.
47. Correa CR, Litt HI, Hwang WT, et al. Coronary artery findings after left-sided compared with right-sided radiation treatment for early-stage breast cancer. *J Clin Oncol* 2007;25:3031–7.
48. Tudor GS, Harden SV, Thomas SJ. Three-dimensional analysis of the respiratory interplay effect in helical tomotherapy: baseline variations cause the greater part of dose inhomogeneities seen. *Med Phys* 2014;41:031704-1–13.
49. Marks LB, Bentzen SM, Deasy JO, et al. Radiation dose–volume effects in the lung. *Int J Radiat Oncol Biol Phys* 2010;76:S70–6.
50. Okunieff P, Morgan D, Niemierko A, et al. Radiation dose-response of human tumors. *Int J Radiat Oncol Biol Phys* 1995;32:1227–37.
51. Horton JK, Halle JS, Chang SX, et al. Comparison of three concomitant boost techniques for early-stage breast cancer. *Int J Radiat Oncol Biol Phys* 2006;64:168–75.
52. Hedin E, Bäck A. Influence of different dose calculation algorithms on the estimate of NTCP for lung complications. *J Appl Clin Med Phys* 2013;14:127–39.